JPE 11-2-2

Control of a Bidirectional Z-Source Inverter for Electric Vehicle Applications in Different Operation Modes

Omar Ellabban†, Joeri Van Mierlo*, and Philippe Lataire*

†* Dept. of Electrical Engineering and Energy Technology, Vrije Universiteit Brussel, Brussels, Belgium

Abstract

This paper proposes two control strategies for the bidirectional Z-source inverters (BZSI) supplied by batteries for electric vehicle applications. The first control strategy utilizes the indirect field-oriented control (IFOC) method to control the induction motor speed. The proposed speed control strategy is able to control the motor speed from zero to the rated speed with the rated load torque in both motoring and regenerative braking modes. The IFOC is based on PWM voltage modulation with voltage decoupling compensation to insert the shoot-through state into the switching signals using the simple boost shoot-through control method. The parameters of the four PI controllers in the IFOC technique are designed based on the required dynamic specifications. The second control strategy uses a proportional plus resonance (PR) controller in the synchronous reference frame to control the AC current for connecting the BZSI to the grid during the battery charging/discharging mode. In both control strategies, a dual loop controller is proposed to control the capacitor voltage of the BZSI. This controller is designed based on a small signal model of the BZSI using a bode diagram. MATLAB simulations and experimental results verify the validity of the proposed control strategies during motoring, regenerative braking and grid connection operations.

Key Words: Bidirectional Z-source Inverter, Grid interface, Indirect field-oriented control, Regenerative braking

I. INTRODUCTION

With increasing oil prices and global warming, automobile manufacturers are producing more hybrid electric vehicles (HEV) and electric vehicles (EV). In hybrid and electric vehicles, the motor drive comprised of an electric motor, a power converter and an electronic controller, is the core of the EV propulsion system. Many research efforts have been focused on developing new DC/DC converters and inverters suitable for hybrid and electric vehicles applications.

There are two basic configurations for power converters used in HEV: one is a traditional PWM inverter powered by a battery as shown in Fig. 1, the other is an inverter plus a DC/DC converter as shown in Fig. 2. Usually a bidirectional DC/DC converter is used. It acts as a boost converter during motoring operation to drive the traction motor for high speed and high torque and it works as a buck converter to capture regenerative braking energy. As a result, bidirectional power transfer is desirable and leads to improvements in the HEV's efficiency for transient drive cycles. The battery voltage variations in HEVs can be as large as 50% and depend on the battery type. With this voltage range, a traditional PWM inverter has to be oversized to handle the full voltage and twice the current at 50% of the battery voltage to output full power. This increases the cost of the inverter. A DC/DC boosted PWM inverter can minimize the stress of the inverter with an extra bidirectional DC/DC stage; however, this increases the system cost and complexity while reducing reliability [1].

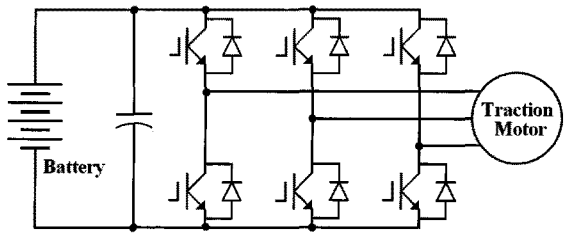

Fig. 1. Traditional PWM inverter for HEV applications.

The Z-source inverter (ZSI), as shown in Fig. 3, is an emerging topology of power electronics converters with very interesting properties such as buck-boost characteristics and single stage conversion. It has a niche for automotive applications to overcome the above mentioned problems. It can: produce any desired AC output voltage, even one greater than the input voltage; provide ride-through during voltage sags without any additional circuits; improve the power factor and reduce the harmonic current and the common-mode voltage [2].

The above features make the ZSI fed adjustable speed drive (ASD) systems highly desirable and reliable when compared to voltage source inverter (VSI) fed ASDs. A ZSI for ASD

‡ Manuscript received May 10, 2009; revised Dec. 30, 2010
† Corresponding Author: omar.ellabban@vub.ac.be
TeX: +32-2-629-29-92, Fax: +32-2-629-36-20, Vrije Univ. Brussel
* Dept. of Electrical Engineering and Energy Technology, Vrije Universiteit Brussel, Belgium

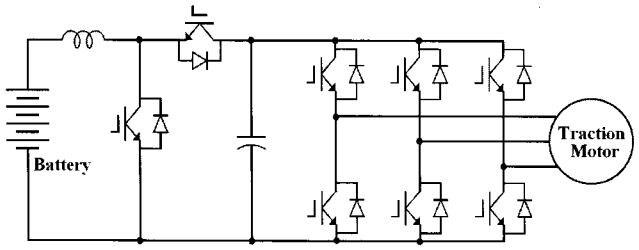

Fig. 2. DC/DC boosted PWM inverter for HEV applications.

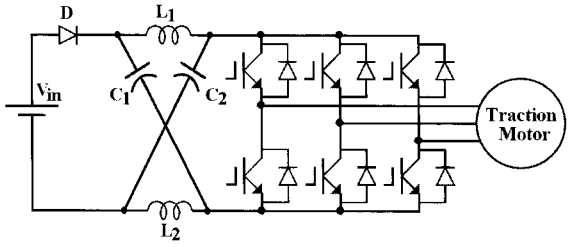

Fig. 3. Basic Z-Source inverter for HEV applications.

systems has been proposed in [3] where the features and advantages of the ZSI fed induction motor systems over the traditional VSI based systems were outlined. In [4], a current mode integrated control technique (CM-ICT) using a modified voltage space vector modulation (MSVM) for ZSI fed induction motor drives has been proposed using two control loops. An outer voltage loop controls the motor line voltage through a PI controller and an inner current loop regulates the motor phase current through a PI controller and a limiter to provide the reference voltage for the MSVM block. The PI controllers were tuned using the Ziegler-Nichols method and the motor line voltages and currents were sensed to provide feedback signals. In this method, the DC-link voltage is not controlled. In addition, there is no speed or torque control for the induction motor.

A bidirectional ZSI (BZSI) topology has been proposed in [5], where the basic ZSI topology was changed into a bidirectional ZSI topology by replacing the input diode, D, with a bidirectional switch, S7, as shown in Fig. 4. The BZSI is able to exchange energy between AC and DC energy storages in both directions. Also, the BZSI is able to completely avoid the undesirable operation modes when the ZSI operated under a small inductance or a low load power factor [6]. A BZSI has been used for an ASD in [7], where a feedforward compensator was designed to reject the DC-link voltage ripples. Another BZSI topology for EV was proposed in [8], where the proposed converter works as a ZSI for motoring operation and performs as a current-fed Z-source DC/DC converter during reverse power flow. However, this converter has an increased switch number and complicated operation modes. A bidirectional Z-source nine-switch inverter (BZS-NSI) was proposed in [9] to replace the conventional HEV configuration with a bidirectional DC/DC converter and two VSI inverters for power transfer among a battery, an electric motor and an electric generator. A V/F open loop control combined with pulse amplitude modulation PWM (PAM/PWM) is used to control an ASD based on the high-performance ZSI in [10].

The battery charger is one of the main electrical units for electric vehicles (EV) and plug-in hybrid vehicles (PHEV).

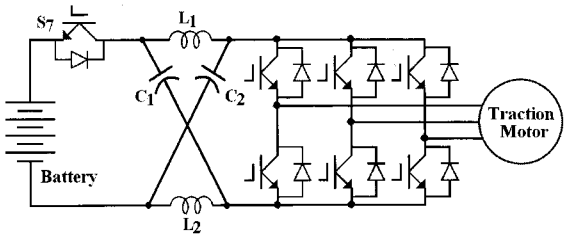

Fig. 4. Bidirectional Z-Source inverter for HEV applications.

In recent years, off-board chargers for fast charging and on-board chargers for slow charging have been developed. In [11], different power electronics topologies used for battery utility connection were reviewed, where a two-stage topology consisting of a DC/AC inverter with a bidirectional DC/DC converter is used for bidirectional power flow and a transformer is used for isolation or a high voltage conversion ratio.

To achieve good performance for both of the DC boost and the AC output voltage in a ZSI, several closed-loop control methods have been proposed [12]–[16]. The DC boost control can be achieved by different methods, including: controlling the Z-network capacitor voltage [12], [13], indirect controlling of the dc-link voltage [14] and direct controlling of the dc-link voltage [15], [16], where a single loop control was used.

The major types of electric traction motors adopted for HEVs include the DC motor, the induction motor (IM), the permanent magnet (PM) synchronous motor, and the switched reluctance motor (SRM). Induction motors have many advantages when compared with other motor types, such as: size, efficiency, cost, life span and maintainability. According to the comparative study presented in [17], the IM seems to be the most widely adapted candidate for the electric propulsion of HEVs.

In this paper, indirect field oriented control (IFOC) is proposed for controlling the speed of an induction motor fed by a bidirectional Z-source inverter (BZSI) for battery electric vehicle (BEV) applications during motoring and regenerative braking operations. Also, this paper presents the application of a proportional plus resonance (PR) controller for controlling the AC current of a bidirectional battery grid connection during battery charging/discharging mode. In addition, this paper proposes a dual loop capacitor voltage control designed based on a small signal model of the BZSI to be used in both control strategies. Using a BZSI with the proposed control strategies as a single stage converter, instead of a two stage converter (bidirectional DC/DC converter and VSI), gives some advantages such as: reduced cost and higher efficiency due to a lower component number as well as reduced volume and easier control implementation.

II. Operation Modes And Modeling Of A Bidirectional ZSI

A BZSI can be obtained by replacing the input diode, D, with a bidirectional switch, S_7, to allow a bidirectional power flow. S_7 operates during the regenerative mode in the same way as the diode during the inverter mode, and its gate signal is the complement of the shoot-through signal. A bidirectional ZSI operates in seven different operation modes from the

current relationships [5]. However, considering the voltage relationships these seven operation modes are generalized to two modes as a basic ZSI. Therefore, all the relationships described in detail in [2] about the Z-source network capacitor voltage, the shoot-through duty ratio, and the output voltage hold true for a BZSI.

$$\frac{d}{dt}\begin{bmatrix}\tilde{i}_L(t)\\ \tilde{v}_c(t)\\ \tilde{i}_l(t)\end{bmatrix}=\begin{bmatrix}0 & \frac{2D_0-1}{L} & 0\\ \frac{1-2D_0}{C} & 0 & \frac{-(1-D_0)}{C}\\ 0 & \frac{2(1-D_0)}{L_l} & \frac{-R_l}{L_l}\end{bmatrix}\cdot\begin{bmatrix}\tilde{i}_L(t)\\ \tilde{v}_c(t)\\ \tilde{i}_l(t)\end{bmatrix}+\begin{bmatrix}\frac{1-D_0}{L}\\ 0\\ \frac{-(1-D_o)}{L_l}\end{bmatrix}\cdot\tilde{v}_{in}(t)+\begin{bmatrix}\frac{2V_C-V_{in}}{L}\\ \frac{-2I_L+I_l}{C}\\ \frac{-2V_C+V_{in}}{L_l}\end{bmatrix}\cdot\tilde{d}_0(t) \tag{1}$$

$$\begin{aligned}V_C&=\frac{1-D_o}{1-2D_0}V_{in}\\ I_L&=\frac{1-D_o}{1-2D_0}I_l\\ I_l&=\frac{V_C}{R_l}\end{aligned} \tag{2}$$

$$G_{vd}(s)=\frac{(-2I_L+I_l)L_lLs^2+[(-2I_L+I_l)R_lL+(1-D_0)(2V_C-V_{in})L+(1-2D_0)(2V_c-V_{in})L_l]s+(1-2D_0)(2V_c-V_{in})R_l}{L_lLCs^3+R_lLCs^2+[2L(1-D_0)^2+L_l(2D_0-1)^2]s+R_l(2D_0-1)^2} \tag{3}$$

$$G_{id}(s)=\frac{(2V_C-V_{in})L_lCs^2+[R_lC(2V_C-V_{in})+(1-2D_0)(-2I_L+I_l)L_l]s+(1-D_0)(2V_C-V_{in})+(1-2D_0)(-2I_L+I_l)R_l}{L_lLCs^3+R_lLCs^2+[2L(1-D_0)^2+L_l(2D_0-1)^2]s+R_l(2D_0-1)^2}. \tag{4}$$

A third order model, with the following state variables: capacitor voltage v_c, inductor current i_L, and load current i_l, of a BZSI can be illustrated by simplifying the ac side circuit to an equivalent dc RL load, Z_l, in parallel with a switch S2 while the bidirectional switch S_7 is represented by a switch S1, as shown in Fig. 5 [18]. Where, R_l is calculated by the power balance as: $R_l=8|Z_{ac}|/3\cos\varphi$, $Z_{ac}=R_{ac}+j\omega L_{ac}$ and L_l is determined so that the time constant of the dc load is the same as the ac load. The two basic operations of the BZSI are shown in Fig. 6. In Mode 1, the energy transferred from the source to the load is zero because the load side and the source side are decoupled by the shoot-through state. In Mode 2, the real energy transfer between the source and the load occurs. Equations (1)-(4) represent: the third order small signal model, the steady state values of the state variables, the control of the capacitor voltage $G_{vd}(s)$ and the control of the inductor current $G_{id}(s)$ small signal transfer functions of the BZSI, where V_{in}, R_l, L_l, I_L, V_C, I_l, D_0 are the input battery voltage, the equivalent dc load resistance, the equivalent dc load inductance, and the steady state values of the inductor current, the capacitor voltage, the load current and the shoot-through duty ratio at a certain operating point, respectively, while L,C are the Z-network capacitor and inductor values.

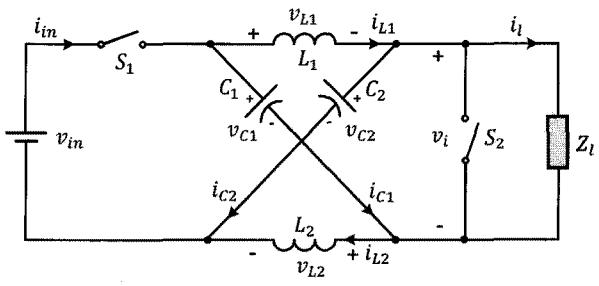

Fig. 5. A simplified equivalent circuit for the BZSI.

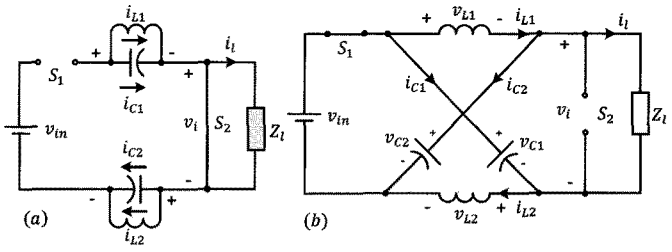

Fig. 6. The basic two equivalent operation modes. (a) Shoot-through state. (b) Non shoot-through state.

III. Capacitor Voltage Control

This paper proposes a dual loop controller, as shown in Fig. 7, to control the capacitor voltage v_c of a BZSI. The proposed control generates a shoot through duty ratio d_0 by controlling both the inductor current i_L and the capacitor voltage v_c of the BZSI. The proposed controller gives better performance during transient and steady state operations. The loop gains for inner current loop $T_i(s)$and outer voltage loop $T_v(s)$ can be expressed as:

$$\begin{aligned}T_i(s)&=G_{ci}(s)G_M(s)G_{id}(s)\\ T_v(s)&=\frac{G_{cv}(s)G_M(s)G_{vd}(s)}{1+T_i(s)}\end{aligned} \tag{5}$$

where $G_{cv}(s)$ and $G_{ci}(s)$ are the transfer functions for the outer voltage loop and the inner current loop controllers. $G_M(s)$ is the shoot-through to the modified modulation signal transfer function and it is expressed by [12]:

$$G_M(s)=\frac{D_0(s)}{v'_m(s)}=\frac{2}{V_{tri}} \tag{6}$$

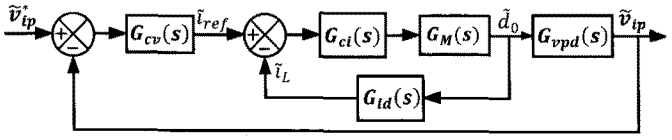

Fig. 7. Dual loop capacitor voltage control of the BZSI.

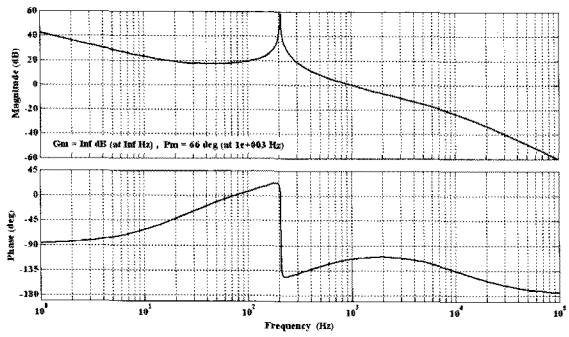

(a)

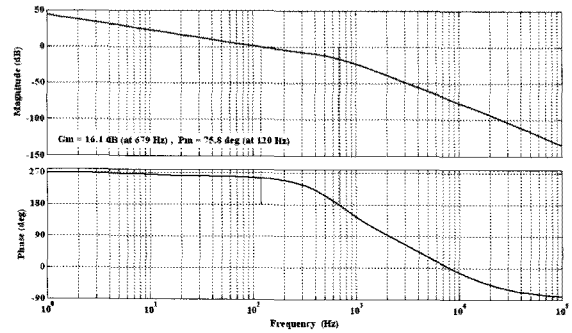

(b)

Fig. 8. Frequency plots for the dual loop capacitor voltage control.

where V_{tri} is the amplitude of the triangle carrier signal. For the outer voltage and the inner current loops, a two pole and one zero controller has been designed to compensate the low-frequency loop gain and improve the phase margin, whose transfer function is:

$$G_c(s) = G_{c0}\frac{(1+s/\omega_z)}{s(1+s/\omega_p)}. \tag{7}$$

To design this controller: first, a new crossover frequency f_c is chosen; then, an arbitrary value for the phase margin is chosen; then, the pole and zero frequencies are calculated as:

$$f_z = f_c\sqrt{\frac{1-\sin(\theta)}{1+\sin(\theta)}}, \qquad f_p = f_c\sqrt{\frac{1+\sin(\theta)}{1-\sin(\theta)}} \tag{8}$$

finally, the controller gain is given by:

$$G_{c0} = \left|\frac{1}{T(s)}\right|_{f=f_c}. \tag{9}$$

Fig. 8 shows bode plots for the current loop and voltage loops gain, respectively, using the system parameters listed in Table I in the Appendix. The plots indicate that the current loop gain has a crossover frequency of 1 kHz, with a phase margin of 66°, as shown in Fig. 8(a), and the resulting outer voltage loop has a crossover frequency of 120 Hz and a phase margin of 76°, as shown in Fig. 8(b).

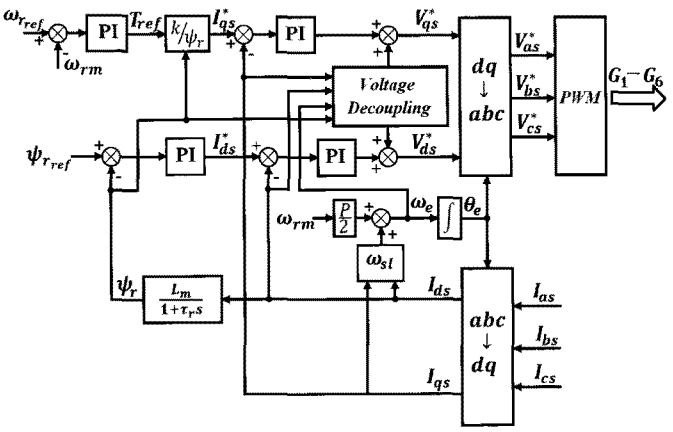

Fig. 9. Block diagram of the IFOC of an induction motor.

IV. Motoring And Regenerative Operation Modes Control

In order to achieve high dynamic performance in an induction motor drive application, vector control is often applied. Vector control makes AC drives behave like DC drives by independently controlling the flux and the torque of the motor [19]-[21]. In indirect field-oriented control (IFOC), the rotating reference frame is rotating at a synchronous angular velocity ω_e. This reference frame allows the three phase currents to be viewed as two dc quantities under steady state conditions. The q-axis component is responsible for the torque producing current, i_{qs}, and the d-axis is responsible for the field producing current, i_{ds}. These two vectors are orthogonal to each other so that the field current and the torque current can be controlled independently.

Fig. 9 shows a block diagram of the IFOC technique for an induction motor. The q-axis component of the stator reference current,i^*_{qs}may be computed using the reference torque, T_{ref}, which is the output of a PI speed controller, as:

$$i^*_{qs} = \frac{2}{3}\frac{2}{p}\frac{L_r}{L_m}\frac{T_{ref}}{\psi_r} \tag{10}$$

where ψ_r is the estimated rotor flux, which is given by:

$$\psi_r = \frac{L_m}{\tau_r s+1} i_{ds}. \tag{11}$$

where L_m, L_r and τ_r are the magnetization inductance, the rotor inductance, and the rotor time constant, respectively. The d-axis component of the stator reference current, i^*_{ds}, may also be obtained by using the reference input flux, $\psi_{r_{ref}}$, which is the output of a PI flux controller, as:

$$i^*_{ds} = \frac{\psi_{r_{ref}}}{L_m}. \tag{12}$$

By using the rotor speed,ω_{rm}, and the slip frequency, ω_{sl}, which is given by:

$$\omega_{sl} = \frac{1}{\tau_r}\frac{i^*_{ds}}{i^*_{qs}} \tag{13}$$

the angle of the rotor flux,θ_e, may be evaluated as:

$$\theta_e = \int(\omega_e + \omega_{rm})dt. \tag{14}$$

Proportional integral controllers regulate the stator voltages, v^*_{ds} and v^*_{qs}, to achieve the calculated reference stator currents,

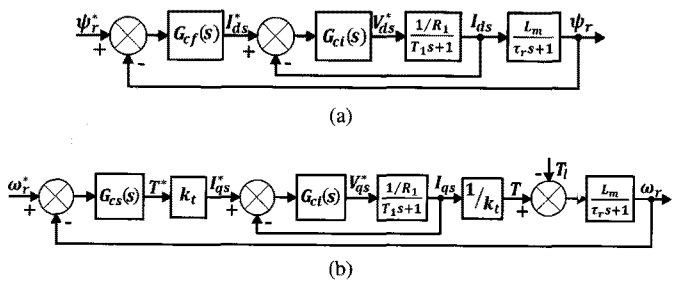

Fig. 10. Flux and speed regulation block diagrams.

TABLE II
PI CONTROLLERS PARAMETERS EQUATIONS

Speed controller	$k_{p_s} = 2J\xi\omega_n - F$ $k_{i_s} = J\omega_n^2(2\xi^2 - 1)$
Flux controller	$k_{p_f} = (2\tau_r\xi\omega_n - 1)/L_m$ $k_{i_f} = \tau_r\omega_n^2(2\xi^2 - 1)/L_m$
Current controller	$k_{p_i} = 2R_1T_1\xi\omega_n - R_1$ $k_{i_i} = R_1T_1\omega_n^2(2\xi^2 - 1)$

i_{ds}^* and i_{qs}^*. The required voltage is then synthesized by the inverter using pulse width modulation (PWM). During motor operation the actual rotor resistance and inductance can vary. The resulting errors between the values used and the actual parameters cause an incomplete decoupling between the torque and the flux. In order to compensate for this incomplete decoupling, the values of compensation voltages are added to the output of the current controllers. This voltage compensation can improve the performance of the current control loops. The compensations terms are given by [20]:

$$\begin{aligned} v_{dsc} &= -\omega_e\sigma L_s i_{qs}^* \\ v_{dsc} &= \omega_e\sigma L_s i_{ds}^* + \frac{L_m}{L_r}\omega_r\psi_r \end{aligned} \quad (15)$$

The parameters of four PI controllers are calculated based on the block diagram shown in Fig. 10 [21]. They are not optimized using practical swarm optimization (PSO) as in [22] or tuned by trial and error. Table II shows the derived equations used to calculate these parameters, where ξ, $\omega_n$are the desired damping and dynamics response specifications, while $R_1 = R_s + R_r \cdot L_m^2/L_r^2$ is the combined motor resistance, and $T_1 = \sigma L_s/R_1$ is the current model time constant.

Fig. 11 shows the entire closed loop system containing: the input battery, the BZSI, the capacitor voltage control and the IFOC speed control, where the capacitor voltage control generates the shoot-through duty ratio and the IFOC generates the modulation index according to the operating conditions.

V. GRID CHARGING/DISCHARGING OPERATION MODE CONTROL

The main goals of the grid interface control technique are to ensure the required power in a three phase grid during battery discharge and to provide enough charge power during battery charging. By regulating the capacitor voltage and hence the dc-link voltage at a certain level, the Z-source inverter can be conveniently regulated by a current control method. Thus, an effective algorithm for the AC current control is needed. The controller for the AC side of the inverter was designed in the stationary reference frame using a proportional plus resonance controller (PR), its transfer function is [23]:

$$G_c(s) = K_p + \frac{2K_i s}{s^2 + \omega_0^2} \quad (16)$$

where K_p, K_i and ω_0 are the proportional gain, the integral gain and the angular frequency at the fundamental frequency. The resonance controller gives an infinite gain at the fundamental frequency which results in integral action at that particular frequency while removing the steady state error. Fig. 12, shows the control strategy of a grid connected bidirectional ZSI. Where P* is the required power injected into or drawn from the grid. Using this power and the measured grid voltage components in the stationary reference frame, v_d, v_q, the reference currents are calculated by [24]:

$$i_d^* = \frac{v_d}{v_d^2 + v_q^2} \cdot P^*, \qquad i_q^* = \frac{v_q}{v_d^2 + v_q^2} \cdot P^*. \quad (17)$$

The phase angle θ of the grid voltage is detected by a PLL and is used in the abc-dq and dq-abc transformations. Two PR controllers are used to control the d-q axis output current components. The output of these controllers is transformed from dq to abc to generate the modulation signals, as shown in Fig. 12.

VI. SIMULATION RESULTS

In order to verify the proposed control strategies during different operation modes, two simulation models were carried out using MATLAB/SIMULINK software, with the parameters listed in Table I in the Appendix. The first model is used to verify the proposed speed control strategy during the motoring and regenerative braking operation modes of a 15 kW induction motor fed by a BZSI. The second model is used to verify the proposed control strategy of a grid connected BZSI during the charging/discharging operation mode with an active power of up to 15 kW. In both models the simple boost shoot-through control method is used.

Figs. 13-16 show the BZSI fed induction motor response during the motoring and regenerative braking operation modes. The system is operated in different operation modes, as shown in Fig. 13: the acceleration mode with the rated torque during the time interval 0-0.2 sec, the steady state operation mode with the rated torque and the rated speed during the time interval 0.2-0.6 sec, the overloaded transient mode with 120% of the rated torque and the rated speed during the time interval 0.6-1 sec, the deceleration transient mode from the rated speed to half of the rated speed with the rated torque during time interval 1-1.2 sec, the light load transient mode with half the rated load and half the rated speed during the time interval 1.2-1.6 sec, the regenerative braking mode during the time interval 1.6-1.8 sec and the standstill mode during the time interval 1.8-1.9 sec. Fig. 14 shows reference and the actual Z-network capacitor voltages, where the capacitor voltage is controlled to be 653 V, and the dc link voltage changes, the shoot-through duty ratio which is generated from the capacitor voltage control, the modulating signal which is generated from the IFOC control as well as the reference and actual Z-network inductor currents. Fig. 15 shows the battery voltage, the current and the SOC as well as their

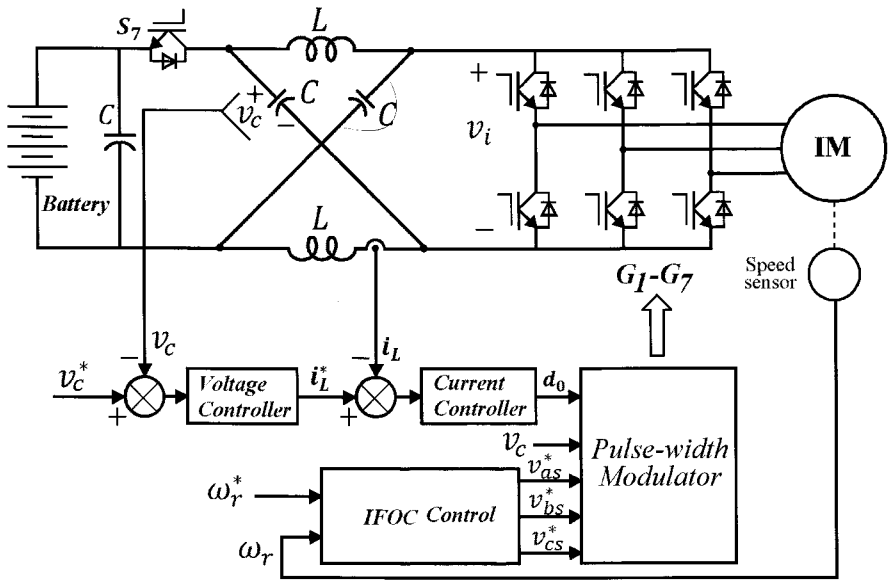

Fig. 11. Closed loop speed control of three phase induction motor fed by a BZSI during motoring and regenerative operation modes.

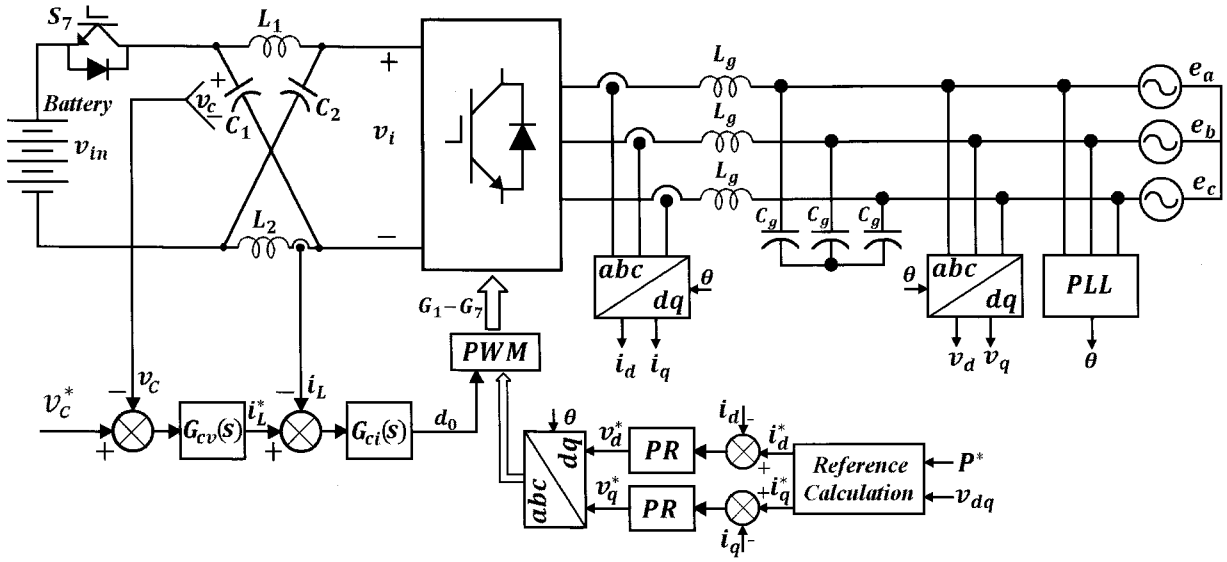

Fig. 12. Control strategy for the grid connected BZSI during charging/discharging mod.

variations during the above mentioned operation modes. Fig. 16 shows the battery power and the motor's electric and mechanical powers for the same operation modes. Figs. 17-19 show the grid connected BZSI during charging/discharging operation mode. The simulation model is tested for one sec in two different operation modes: the battery charging from the grid during the time interval 0-0.5 sec and the battery discharging to the grid during the time interval 0.5-1 sec. Fig. 17 shows the battery SOC, current and voltage, where the SOC increases during battery charging (negative battery current) and decreases during battery discharging (positive battery current). Fig. 18 shows the Z-network capacitor voltage and the inductor current during the battery charging/discharging mode. Fig. 19 shows the grid voltage and current during the transition between the charging/discharging operation modes at t=0.5 sec.

VII. Experimental Results

In order to verify the simulation results, a prototype of a 30 kW ZSI is designed and implemented using the parameters in Table III in the Appendix, as shown in Fig. 20, to drive a 19 kW induction motor. For the realization of the proposed control methods an evaluation board eZdsp^{TM} F2808 based on a TMS320F2808 Digital Signal Processor (DSP) has been chosen [25]. The eZdsp evaluation board is connected to a PC using a USB cable and the PC has MATLAB, Real Time workshop (RTW) and code composer studio (CCS) installed on it for automatic code generation and real time control. Figs. 21-27 show the experimental results. Fig. 21 shows the switching signal for phase A of the ZSI, where the shoot-through state is indicated. Figs. 22 and 23 show the induction motor line voltages and the phase currents when the motor draws 10 A (25% rated load) and 25 A (65% rated load) from the ZSI, respectively. Figs. 24 and 25 show, the input

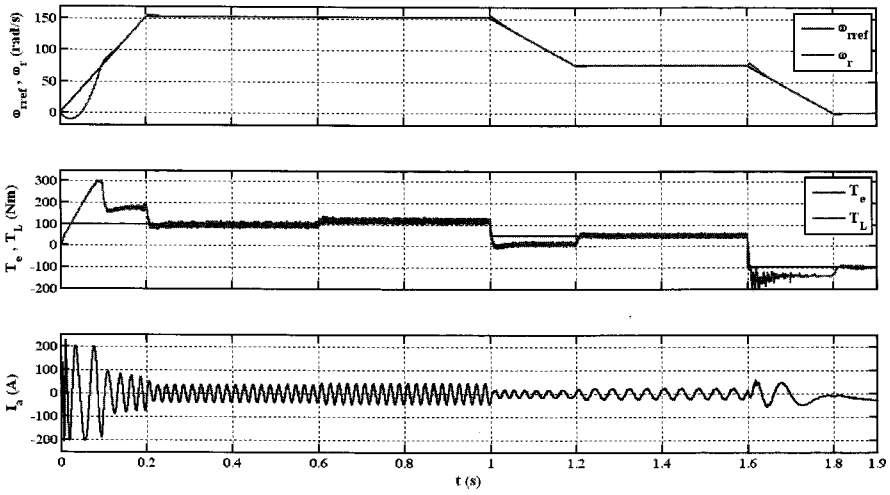

Fig. 13. Motor response during motoring and regenerative braking operation modes.

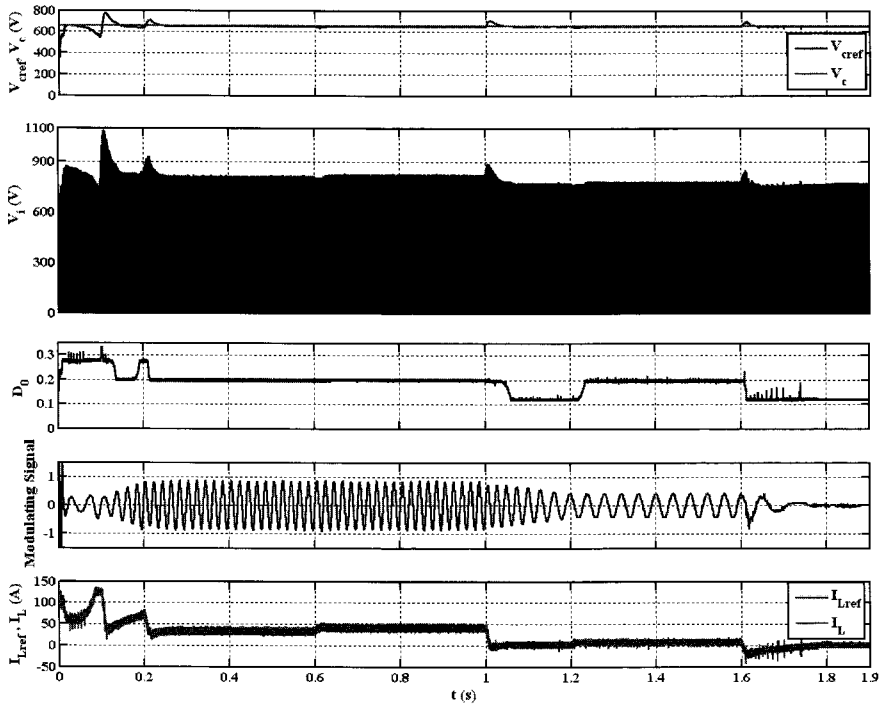

Fig. 14. BZSI response during motoring and regenerative braking operation modes.

voltage, the capacitor voltage, the dc-link voltage and the inductor current of the ZSI at 25% and 65% of the rated load, respectively. As shown in Figs. 24-25, the capacitor voltage is controlled to be 300 V even when the motor load changes from 25% to 65% of the rated load. Fig. 26 shows the input voltage, the capacitor voltage, the dc-link voltage and the inductor of the ZSI in the switching frequency at 65% of the rated load. Fig. 27 shows the steady state speed and torque of the induction motor at 65% of the rated load.

VIII. Conclusion

This paper proposes two control strategies for bidirectional Z-source inverters for electric vehicle applications. The first control strategy utilizes the indirect field-oriented control (IFOC) method to control the induction motor speed during motoring and regenerative braking operation modes. The second control strategy utilizes a proportional plus resonance (PR) controller to control the AC current for connecting a BZSI to the grid during battery charging/discharging operation mode. In both control strategies the Z-network capacitor voltage is controlled by a dual loop control. The first control strategy is tested during standard (acceleration, steady state, regenerative braking and standstill) and transient (overload, deceleration and light load) modes. The second control strategy is tested during battery charging/discharging operation mode. MATLAB simulations and experimental results verify the validity of the proposed control strategies during different operation modes. The application of a BZSI to battery operated electric vehicles (BEV) can improve their efficiency and reduce their production cost due to a lower component count, since it is a one stage converter with a reduced volume and easier control implementation.

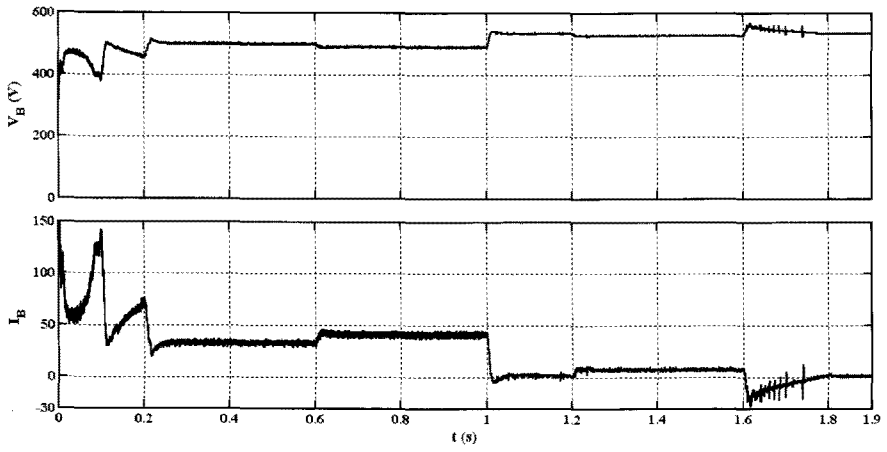

(a)

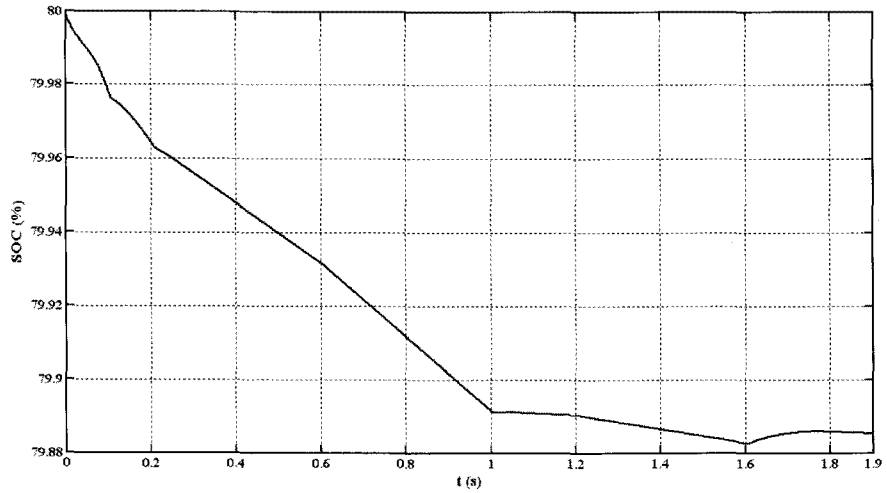

(b)

Fig. 15. Battery voltage and current (a), battery state of charge (SOC) during motoring and regenerative braking operation modes.

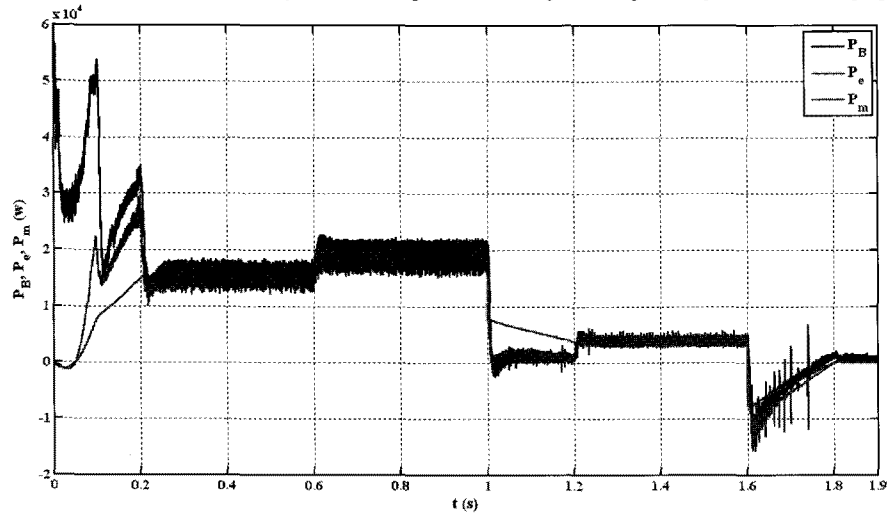

Fig. 16. Battery power and motor electric and mechanical powers during motoring and regenerative braking operation modes.

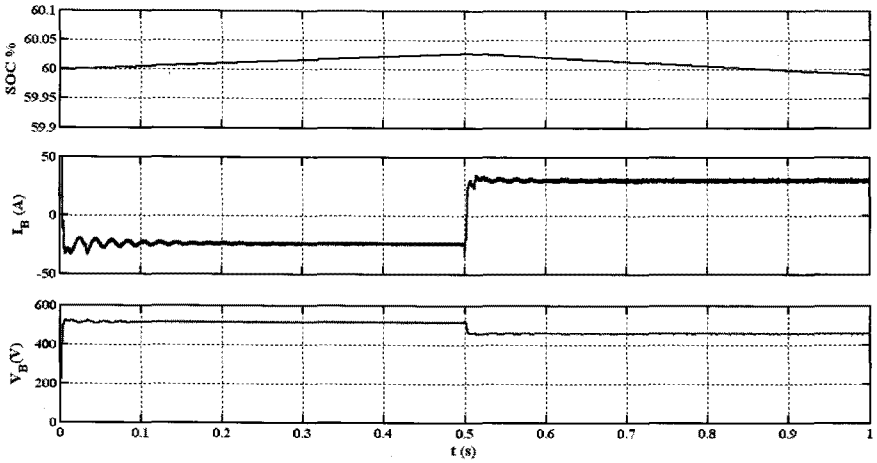

Fig. 17. Battery state of charge (SOC), voltage and current and during grid charging/discharging operation mode.

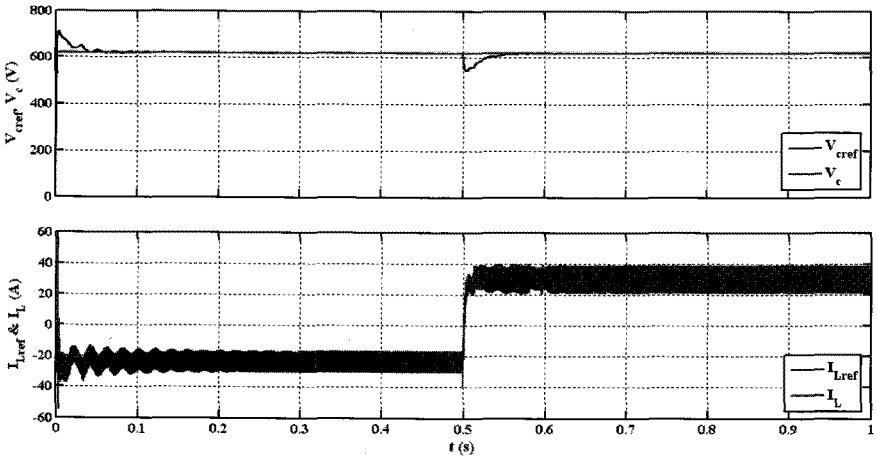

Fig. 18. Z-network capacitor voltage and inductor current and during grid charging/discharging operation mode.

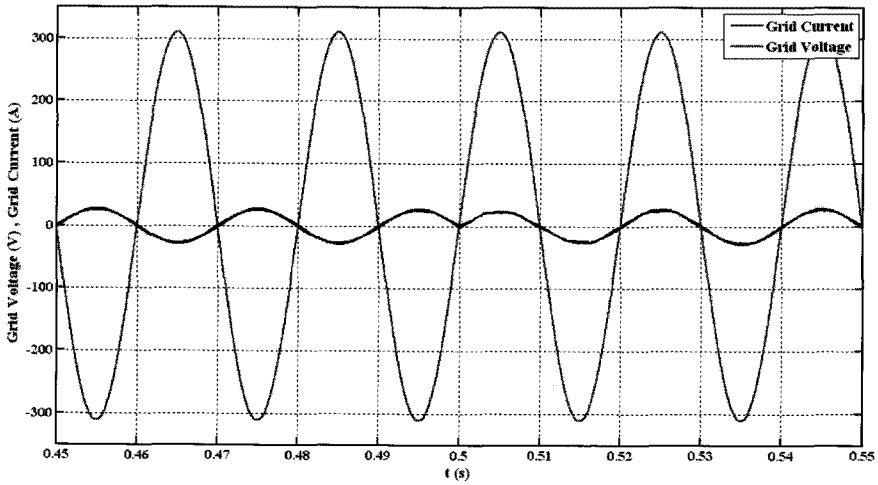

Fig. 19. Grid voltage and current during transition between charging/discharging operation modes.

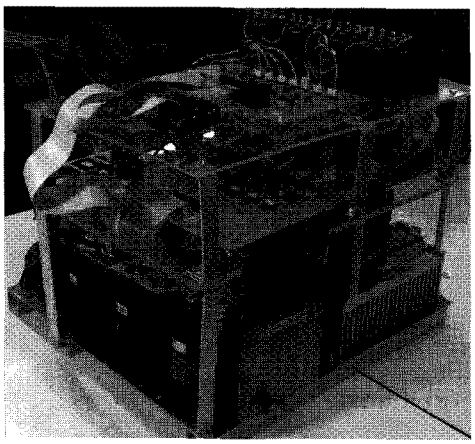

Fig. 20. Experimental setup of a 30 kW ZSI.

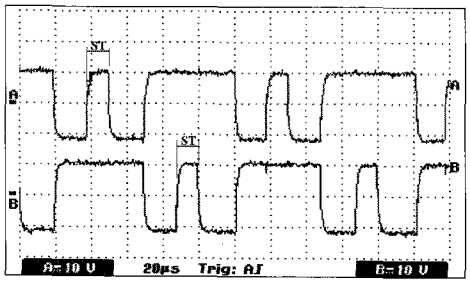

Fig. 21. Switching signal of phase A of the BZSI.

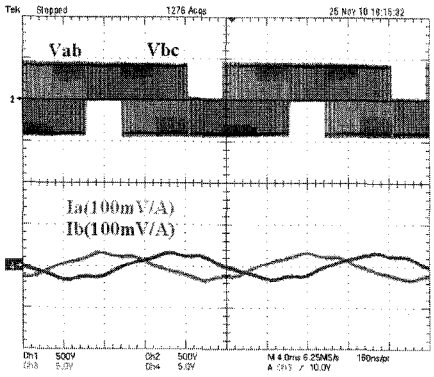

Fig. 22. Motor line voltages and phase currents 25% of the rated load.

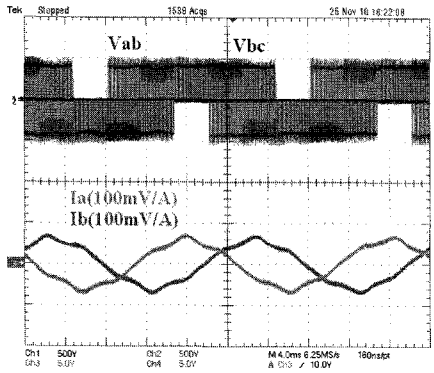

Fig. 23. Motor line voltages and phase currents 65% of the rated load.

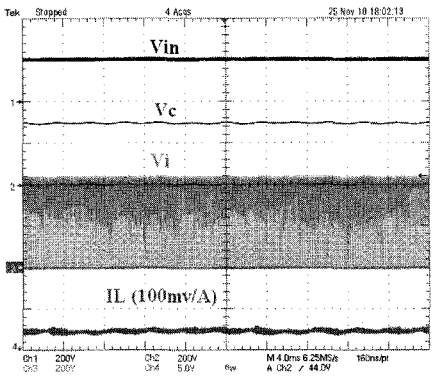

Fig. 24. BZSI waveforms in line frequency at 25% rated load.

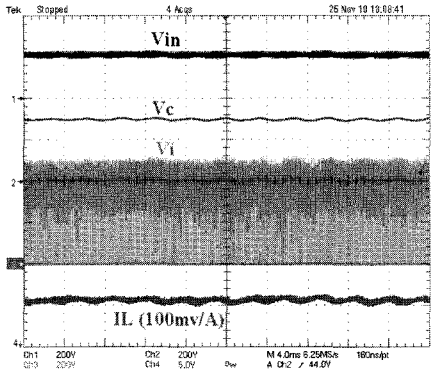

Fig. 25. BZSI waveforms in line frequency at 65% rated load.

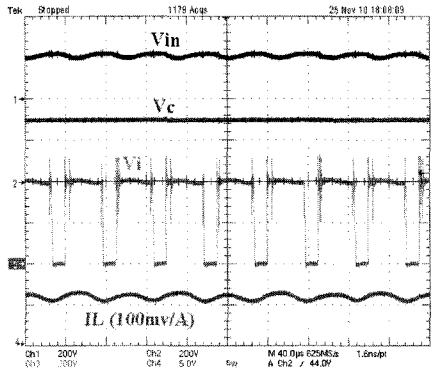

Fig. 26. BZSI waveforms in switching frequency at 65% rated load.

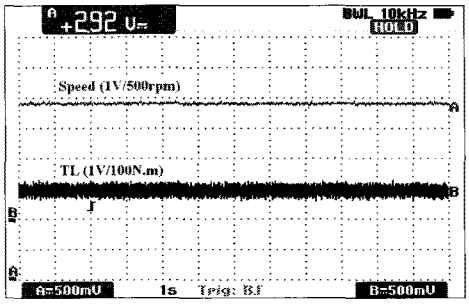

Fig. 27. steady state speed and torque at 65% rated load.

APPENDIX

TABLE I
SIMULATION SYSTEM PARAMETERS

Parameter	Value
BIDIRECTIONAL ZSI PARAMETERS	
Inductance	500 μH
Capacitance	500 μF
Switching frequency	10 kHz
BATTERY PACKAGE PARAMETERS	
Rated capacity	11 Ah
Nominal voltage	490 V
Internal resistance	1.11 Ω
INDUCTION MOTOR PARAMETERS	
Output power	15 kW
RMS line voltage	400 V
Input frequency	50 Hz
No. of poles	4
Stator resistance, Rs	0.2205 Ω
Rotor resistance, Rr	0.2147 Ω
Stator inductance, Lls	0.991 mH
Rotor inductance, Llr	0.991 mH
Mutual inductance, Lm	64.19 mH
Inertia, J	0.102 kg. m2
Fraction factor, J	0.009541 N.m.s
GRID PARAMETERS	
Nominal grid line voltage	380 V
Grid inductance	5 mH

TABLE III
EXPERIMENTAL SYSTEM PARAMETERS

Parameter	Value
ZSI parameters	
Inductance	700 μH
Capacitance	320 μF
Switching frequency	10 kHz
Induction Motor Parameters	
Output power	19 kW
RMS line voltage	380 V
Input frequency	50 Hz
No. of poles	4
Stator resistance, Rs	0.16 Ω
Rotor resistance, Rr	0.21 Ω
Stator inductance, Lls	0.05 H
Rotor inductance, Llr	0.12 H
Mutual inductance, Lm	0.076 H

REFERENCES

[1] M. Shen and F. Z. Peng, "Converter systems for hybrid electric vehicles," *International Conference on Electrical Machines and Systems*, pp. 2004-2010, 2007.

[2] F. Z. Peng, "Z-Source inverter," *IEEE Trans. Ind. Appl.*, pp. 504-510, Vol. 39, No. 2, Mar./Apr. 2003.

[3] F. Z. Peng, X. Yuvan, X. Fang, and Z. Qian, "Z-source inverter for motor drives," *IEEE Trans. Power Eletron.*, Vol. 20, No. 4, pp.857-863, Jul. 2005.

[4] S. Thangaprakashy and A. Krishnan, "Current mode integrated control technique for Z-source inverter fed induction motor drives," *Journal of Power Electronics*, Vol.10, No.3, pp.285-292, May 2010.

[5] X. Haiping, F. Z. Peng, L. Chen, and X. Wen, "Analysis and design of Bi-directional Z-source inverter for electrical vehicles," in *Proc. APEC*, pp.1252-1257, 2008.

[6] M. Shen and F. Z. Peng, "Operation modes and characteristics of the Z-source inverter with small inductance or low power factor," *IEEE Trans. Ind. Eletron.*, Vol. 55, No. 1, pp. 89-96, Jan. 2008.

[7] X. Ding, Z. Qian, S. Yang and F. Z. Peng, "A new feedforward compensation to reject DC-link voltage ripple in bi-directional Z-source inverter ASD system," in *Proc. APEC*, pp. 1809-1813, 2008.

[8] M. Yamanaka and H. Koizum, "A bi-directional Z-source inverter for electric vehicles," *International Conference on Power Electronics and Drive Systems*, pp.574-578, 2009.

[9] S. M. Dehghan, M. Mohamadian, and A. Yazdian, "Hybrid electric vehicle based on bidirectional Z-source nine-switch inverter," *IEEE Trans. Vehicular Technology*, Vol. 59, No. 6, PP.2641-2653, Jul. 2010.

[10] X. Ding, Z. Qian, S. Yang, B. Cuil, and F. Z. Peng, "A new adjustable-Speed Drives (ASD) system based on high-performance Z-source inverter," in *Proc. IAS*, pp.2327-2332, 2007.

[11] S. Chakraborty, B. Kramera, and B. Kroposkia, "A review of power electronics interfaces for distributed energy systems towards achieving low-cost modular design," *Renewable and Sustainable Energy Reviews*, Vol. 13, No. 9, pp. 2323-2335, Jun. 2009.

[12] X. Ding, Z. Qian, S. Yang, B. Cui, and F. Peng, "A PID Control Strategy for DC-link Boost Voltage in Z-source Inverter," in *Proc. APEC*, pp. 1145-1148, 2007.

[13] Q.-V. Tran, T.-W. Chun, H.-G. Kim, and E.-C. Nho, "Minimization of voltage stress across switching devices in the Z-source inverter by capacitor voltage control," *Journal of Power Electronics*, Vol. 9, No.3, pp.335-342, May 2009.

[14] X. Ding, Z. Qian, S. Yang, B. Cui, and F. Z. Peng, "A direct DC-link boost voltage PID-like fuzzy control strategy in Z-source inverter," in *Proc. PESC*, pp. 405-411, 2008.

[15] X. Ding, Z. Qian, S. Yang, B. Cui, and F. Peng, "A direct peak DC-link boost voltage control strategy in Z-source inverter," in *Proc. APEC*, pp. 648-653, 2007.

[16] Y. Tang, J. Wei, and S. Xie, "A new direct peak DC-link voltage control strategy of Z-source inverters," in *Proc. APEC*, pp. 867–872, 2010.

[17] M. Zeraoulia, M. E. H. Benbouzid, and D. Diallo, "Electric motor drive selection issues for HEV propulsion systems: a comparative study," *IEEE Trans. Vehicular Technology*, Vol. 55, No. 6, pp.1756-1764, Nov. 2006.

[18] Jingbo Liu, Jiangang Hu, and Longya Xu, "Dynamic modeling and analysis of z source converter-derivation of AC small signal model and design-oriented analysis," *IEEE Trans. Power Electron.*, Vol. 22, No. 5, pp. 1786-1796, Sep. 2007.

[19] M. A. Mannan, T. Murata, J. Tamura, and T. Tsuchiya, "Indirect field oriented control for high performance induction motor drives using space vector modulation with consideration of core loss," in *Proc. PESC*, Vol. 3, pp. 1449-1454, 2003.

[20] I. K. Bousserhane, A. Hazzab, M. Rahli, M. Kamli, and B. Mazari, "Direct field-oriented control using backstepping strategy with fuzzy rotor resistance estimator for induction motor speed control," *Information Technology and Control*, Vol. 4, No. 4, pp. 403– 411, 2006.

[21] A. Mansouri, M. Chenafa, A. Bouhenna, and E. Etien, "Powerful nonlinear observer associated with field-oriented control of an induction motor," *Int. J. Appl. Math. Comput. Sci.*, Vol. 14, No. 2, 209–220, Jun. 2004.

[22] E. A. Saber, "A novel technique for tuning PI-controllers in induction motor drive systems for electric vehicle applications," *Journal of Power Electronics*, Vol. 6, No.4, pp.322-329, Oct. 2006.

[23] S. Zhang, K.-J. Tseng, D. M. Vilathgamuwa, T. D. Nguyen, and X.-Y. Wang, "Design of a robust grid interface system for PMSG-based wind turbine generators," *IEEE Trans. Ind. Electron.*, Vol. 58, No. 1, pp. 316-328, Jan. 2011.

[24] J.-H. Park, H.-G. Kim, E.-C. Nho, and T.-W. Chun, "Power conditioning system for a grid connected PV power generation using a quasi-z-source inverter," *Journal of Power Electronics*, Vol. 10, No. 1, pp.79-84, Jan. 2010.

[25] Texas Instruments, Inc., "eZdspTM F2808 USB," Technical Reference 2005.

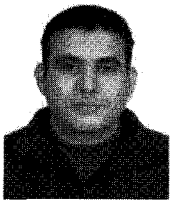

Omar Ellabban was born in Egypt in 1975. He received his B.S. from Helwan University, CityHelwan, Egypt in 1998 and his M.S. from Cairo University, Giza, Egypt in 2005, both in Electric Power and Machines Engineering. He is currently pursuing his Ph.D. in Electrical Engineering at Vrije Universiteit Brussel, Brussels, Belgium. His research interests include motor drives, artificial intelligence, converter design, hybrid electric vehicle control and DSP-based system control.

Joeri Van Mierlo obtained his Ph.D. in Electromechanical Engineering Sciences from Vrije Universiteit Brussel in 2000. He is now a Full Time Professor at this university, where he leads the MOBI - Mobility and Automotive Technology Research Group. His current research interests include the development of hybrid propulsion systems (converters, supercaps, energy-management, etc.) as well as the environmental comparison of vehicles with different kinds of drive trains and fuels (LCA, WTW). He is the author of more than 100 scientific publications. He chairs the EPE chapter on "Hybrid and Electric Vehicles" (www.epe-association.org). He is the Secretary of the Board of the Belgian section of AVERE (ASBE) and is a Board Member of AVERE. He is a Co-Editor of the Journal of Asian Electric Vehicles. He is an active Member of EARPA - the Association of Automotive R&D Organizations. Furthermore he is a Member of Flanders Drive and of VSWB – the Flemish Cooperative on Hydrogen and Fuels Cells. Prof. Van Mierlo is Chairman of the International Program Committee of the International Electric, Hybrid and Fuel Cell Symposium (EVS24).

Philippe Lataire received a degree in Electromechanical Engineering in 1975 and his Ph.D. in 1982, both from Vrije Universiteit Brussel (VUB), Brussels, Belgium. He is presently a Full Time Professor at VUB. His current research interests include electric drives, power electronics and control.